Air Pollution Meteorology

Xiao-Ming Hu[a], Xiaolan Li[b], Bowen Zhou[c], and Ming Xue[a], [a] Center for Analysis and Prediction of Storms and School of Meteorology, University of Oklahoma, Norman, OK, United States; [b] Institute of Atmospheric Environment, China Meteorological Administration, Shenyang, China; and [c] School of Atmospheric Sciences, Nanjing University, Nanjing, China

This is an update of X.-M. Hu, BOUNDARY LAYER (ATMOSPHERIC) AND AIR POLLUTION | Air Pollution Meteorology, Editor(s): Gerald R. North, John Pyle, Fuqing Zhang, Encyclopedia of Atmospheric Sciences (Second Edition), Academic Press, 2015, Pages 227–236, ISBN 9780123822253, https://doi.org/10.1016/B978-0-12-382225-3.00499-0.

Key Points

- Temperature (T) inversion does not work when inferring boundary layer structure for both daytime and nighttime conditions, potential temperature (θ) should be used instead.
- θ profiles are more meaningful than T profiles in air pollution/boundary layer meteorology.
- Low-level jet nose can be used to diagnose nighttime boundary layer top according to the inertial oscillation theory.

Synopsis

Meteorological conditions play important roles in modulating the ambient concentrations of pollutants through different ways, including (1) exerting influences on the formation and fate of pollutants such as ozone and aerosols; (2) dictating the dispersion of pollutants through turbulent mixing and advection. Thus, accurate representation of meteorological conditions is critical for correctly simulating pollution events. Uncertainties are associated with model treatments for various processes in air quality models. Particularly an accurate planetary boundary layer (PBL) scheme is critical for pollution simulation. Methods such as ensemble simulation and parameter estimation could potentially improve air quality simulations.

Graphical Abstract

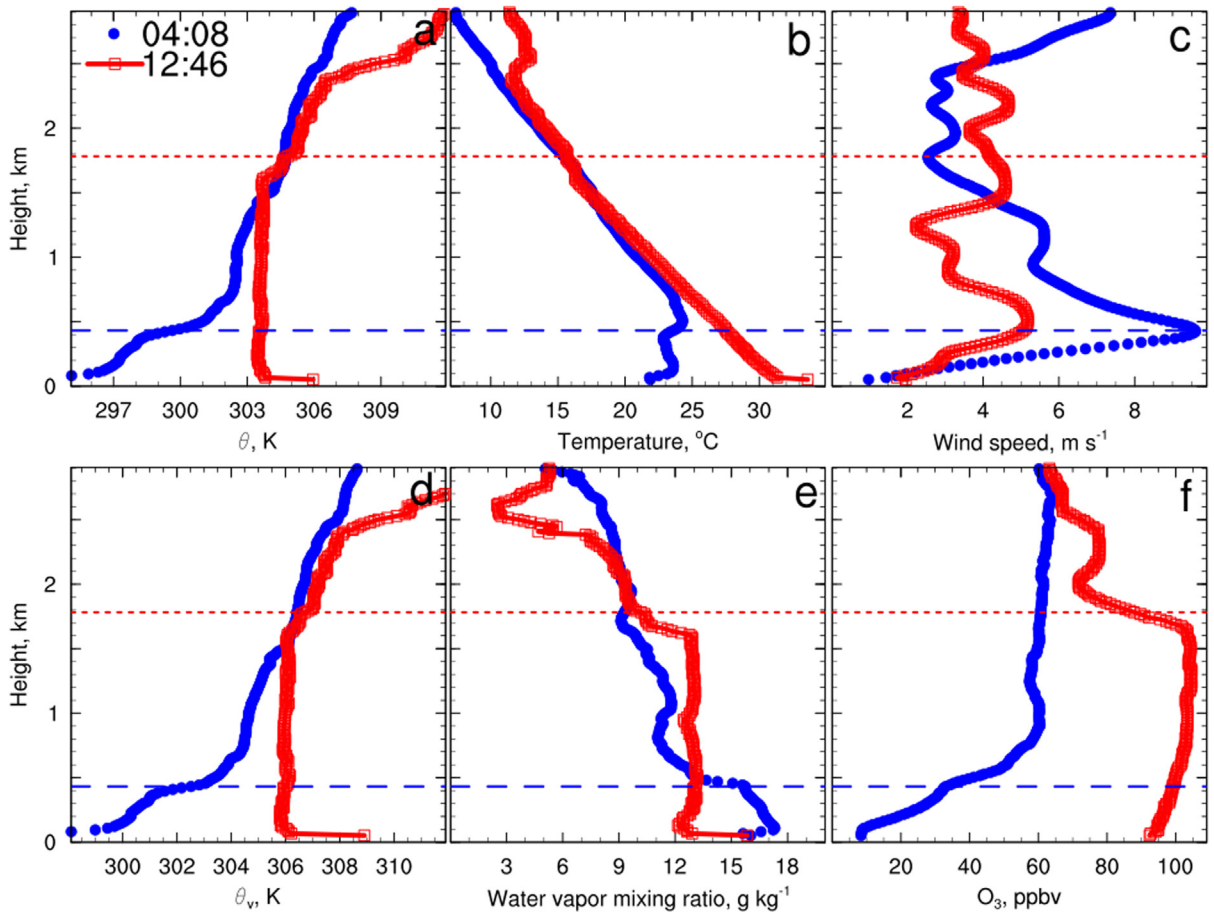

Introduction

The United States (US) Environmental Protection Agency (EPA) set National Ambient Air Quality Standards (NAAQS) for six principal pollutants in 1990s to provide protection for public health and the environment. These six principal pollutants are called "criteria" pollutants, including Carbon Monoxide (CO), Lead, Nitrogen Dioxide (NO_2), ground-level Ozone (O_3), Sulfur Dioxide (SO_2), and Particulate Matter (or aerosols). The NAAQS are periodically reviewed and revised according to the updated science. Among the six criteria air pollutants, the formation of O_3 and aerosols involves the most complicated processes. Ozone is a secondary pollutant, produced from oxides of nitrogen and reactive organic gases in the presence of sunlight. When O_3 reaches critical levels, adverse environmental effects are expected for human health, crops, and natural vegetation. The adverse environmental effects of O_3 were first reported in Los Angeles during 1940s. Now it is realized that O_3 pollution is no longer confined to Los Angeles, and it affects major urban locations in the world. Elevated O_3 concentrations have also been reported in rural and even remote regions. Aerosol particles are ubiquitous in the atmosphere with diameters ranging from a few nanometers to hundreds of micrometers (μm), originating from both primary and secondary sources. Elevated concentrations of aerosols can cause or enhance respiratory, cardiovascular, infectious, and allergic diseases. The primary parameters that determine the environmental and health effects of aerosols are concentration, size, structure, and chemical composition, which are spatially and temporally highly variable.

The overall photochemical O_3 formation mechanism is well known. In the troposphere, O_3 is produced from the photolysis of nitrogen dioxide (Eq. R1) and the subsequent reaction of the ground state oxygen atoms, $O(^3P)$, with molecular oxygen (Eq. R2).

$$NO_2 + h\nu \rightarrow NO + O(^3P) \quad \text{R1}$$

$$O(^3P) + O_2 + M \rightarrow O_3 + M \quad \text{R2}$$

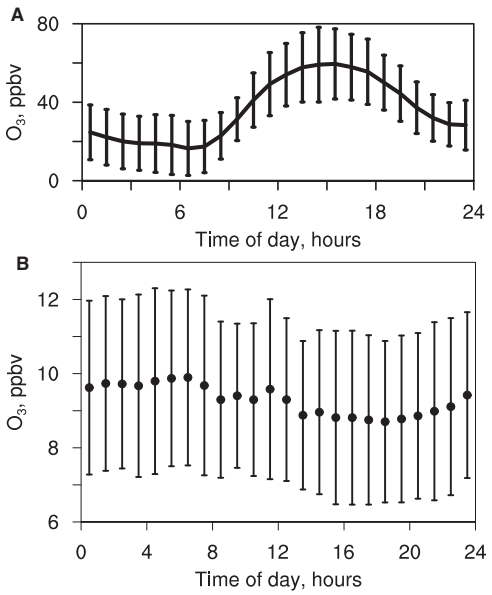

Fig. 1 Mean diurnal variation of O_3 mixing ratio and its standard deviation at (A) Beltsville, Maryland, US during August 2010 and (B) Kwajalein in the equatorial Pacific Ocean during July-September 1999.

where "M" denotes the third body that carries off the excess energy of the reaction. Once formed, O_3 may be removed from the atmosphere through dry deposition process and NO titration reaction (**Eq. R3**)

$$O_3 + NO \rightarrow NO_2 + O_2 \qquad \text{R3}$$

Volatile organic compounds (VOCs) and other species also participate in atmospheric reactions and modulate O_3 concentrations. Ozone has different variability in different regions. In the continental atmospheric boundary layer, where the concentration of nitrogen oxides (NO_x) is relatively high, local photochemical production of O_3 will contribute to the O_3 maximum in the afternoon in the presence of sunlight and high temperature. During the night, O_3 mixing ratios decrease due to NO titration (**Eq. R3**) and dry deposition. **Fig. 1**A shows the typical diurnal variation of continental boundary layer O_3 in Beltsville, Maryland, US during August 2010. In the marine boundary layer, where the concentration of NO_x is relatively low, air chemistry can lead to the destruction of O_3. **Fig. 1**B shows the diurnal variation of O_3 mixing ratio at Kwajalein Atoll situated in the equatorial Pacific Ocean in summer 1999. During the daytime, O_3 photolysis, hydroperoxyl radicals (HO_2), hydroxyl radicals (OH), and bromine atoms (Br) contributed to the destruction of O_3, which led to the observed minimum O_3 levels in the afternoon. The entrainment of O_3-richer air from the free troposphere to the local marine boundary layer provided a recovery mechanism of marine boundary layer O_3 during nighttime (Hu et al., 2010b).

The ambient aerosol particles are characterized by two modes, the fine mode (with a diameter $\leq$2.5 μm) and the coarse mode (with a diameter >2.5 μm). Fine mode aerosol particulate mass is referred to as $PM_{2.5}$, which poses the largest health risks. The aerosol particulate matter may either be directly emitted or formed in the atmosphere, which are referred to as primary and secondary sources respectively. Primary sources of aerosol include combustion, windblown dust, pollen, plant fragments, and sea salt. Secondary aerosols are produced in the atmosphere by photochemical processes and added to the pre-existing particles through the gas/particle mass transfer process (Hu et al., 2008). Most of the mass of $PM_{2.5}$ is composed of secondary aerosol. In some cases, more than 90% of the $PM_{2.5}$ mass may be attributed to secondary aerosol. The chemical formation processes of O_3 and aerosols and their dispersion and transport are modulated by meteorological conditions (Hu et al., 2019b; Zhang et al., 2015).

Effects of Meteorology on Air Pollution

Meteorological conditions modulate the ambient concentrations of pollutants through different ways. Three major influences are summarized below.

Effects of Meteorology on Biogenic Emissions

Biogenic emissions play an important role in regional air quality and global atmospheric chemistry. Isoprene (C_5H_8) is the predominant volatile organic compound (VOC) emitted by vegetation. It is key to the formation of O_3 and aerosols, and affects the lifetime

of other species. Biogenic emissions are controlled by ambient environmental variables, most notably temperature and light. Increase in temperature normally leads to increased isoprene emissions (Zhang et al., 2008).

Effects of Meteorology on the Formation of O_3 and Aerosols

Episodes of high concentrations of surface O_3 usually occur during the summertime in stagnant air under dry, sunny weather conditions. Ozone generally increases with increasing temperature and decreases with increasing relative humidity. Warmer temperature enhances O_3 production through affecting photochemical rate constants and biogenic emissions. Water vapor affects O_3 abundance through its consumption of $O(^1D)$ via the reaction $O(^1D) + H_2O \rightarrow 2OH$.

Meteorological variables affect the formation of precursors of aerosols through modulating the reaction efficiency. Once the semi-volatile precursors of aerosols are formed, meteorological variables also affect the partitioning of those species between the gas phase and aerosols. The partitioning of semi-volatile species depends highly on temperature and relative humidity. Low temperature and high relative humidity favor the partitioning of semi-volatile species into the aerosol phase while high temperature and low relative humidity favor the gas phase (Hu, 2008; Hu et al., 2008).

Effects of Meteorology on Dispersion/Transport of Pollutants

Meteorological processes (e.g., turbulent mixing and advection) dictate the dispersion of pollutants. The ubiquitous turbulence in the lowest part of the troposphere, referred to as the planetary boundary layer (PBL), significantly affects the dispersion/transport of air pollutants and thus the formation and evolution of air pollution episodes. Turbulence is several orders more effective at transporting mass and energy than molecular diffusion. Turbulence is one of the prominent characteristics that differentiates the PBL from the overlying free atmosphere. Turbulence usually consists of eddies of different sizes superimposed on each other, whose scales range from a few millimeters to 100−3000 m that roughly equals the PBL height. Large thermal eddies are primarily driven by surface heating or cloud-top radiative cooling and transport momentum, heat, and constituents throughout the entire PBL. Smaller eddies can be produced by wind shear, breaking shear-instability waves, and shear mixing at the edge of thermals or the breaking down of large eddies through the turbulence cascading processes. Turbulent energy is gradually cascaded from large to small eddies, and is finally dissipated into heat by molecular viscosity.

Different characteristics of PBL with different turbulence in terms of scale and strength dictate the vertical extent and the way pollutants are dispersed. Depending on different PBL structure, pollutants plumes may (1) loop up and down initially and become uniformly distributed vertically eventually, (2) fan out in the horizontal with little vertical dispersion, (3) spread with an almost equal rate in the vertical and horizontal, exhibiting a cone shape.

Characteristics and Structure of the PBL

The PBL is defined as the lowest part of the troposphere with prominent turbulence that is directly influenced by the presence of the earth's surface, and responds to surface forcing within a timescale of about an hour or less through turbulent mixing. The variation of the PBL plays a critical role for dictating the dispersion of pollutants since most pollutants are emitted or formed in the PBL. The PBL depth may vary from tens/hundreds of meters to a few kilometers (km). Over oceans, the PBL depth varies relatively slowly in space and time due to little change of ocean water temperature. The PBL depth varies dramatically over the land. During the daytime, due to surface heating from shortwave radiation, turbulence is generated in the lower 1−2 km above the ground, forming the convective boundary layer (CBL). Vigorous turbulence tends to mix heat, momentum, moisture and pollutants uniformly in the CBL, hence CBL is also called the mixed layer. A stable layer on top of the mixed layer caps the vertical extent of turbulence. This layer is called the entrainment zone due to the vertical entrainment of free tropospheric air into the mixed layer that occurs in this layer. After sunset, turbulence decays in the formerly mixed layer. The upper portion of the formerly mixed layer becomes the residual layer, in which the state variables and concentrations of pollutants remain mostly invariant. The lower portion of the formerly mixed layer is transformed into a stable boundary layer, which is characterized by stably-stratified air with weaker, sporadic turbulence. After sunrise of the following day, the mixed layer starts to grow in depth again.

Static stability and PBL height are two important parameters to characterize the PBL, which dictate the dispersion of atmospheric constituents. The PBL height roughly represents the vertical dilution volume for pollutants. Static stability represents the capability of buoyant potential of air mass and dictates the vertical mixing of air pollutants. Static stability can be categorized into three conditions, depending on the further motion of an air mass under small vertical perturbation. If the motion is accelerating/maintaining/decelerating, the static stability is unstable, neutral, and stable, respectively.

Static stability is commonly examined based on profiles of air temperature (T) or virtual potential temperature (θ_v)

$$\theta_v = \theta \cdot (1 + 0.61 \cdot q - q_l),$$

where θ is the potential temperature, q is the mixing ratio of water vapor, and q_l is the mixing ratio of liquid water in the air. Since air mass T is not conserved and follows dry-adiabatic lapse late ($= 9.8\ ^\circ\mathrm{C\ km^{-1}}$) during vertical displacement, atmospheric static stability can be only inferred by comparing T profile with the slope of dry-adiabatic lapse rate, basically examining whether the slope of the T profile is larger or smaller than $9.8\ ^\circ\mathrm{C\ km^{-1}}$, which is not easy to judge based on a T profile plot with naked eyes. In contrast, θ_v is a conservative quantity when air mass is vertically displaced, which is related to air density, thus buoyancy potential.

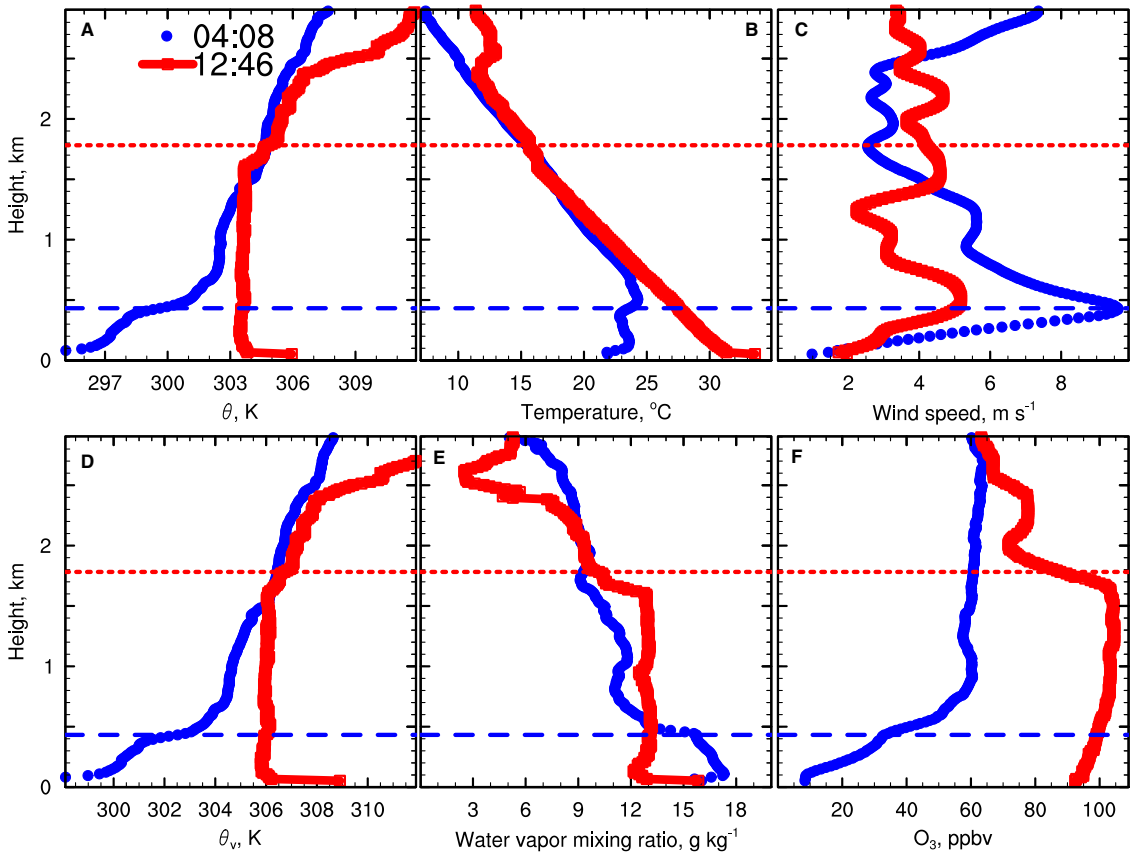

Fig. 2 Profiles of (A) potential temperature (θ), (B) air temperature, (C) wind speed, (D) virtual potential temperature (θ_v), (E) water vapor mixing ratio, and (F) O_3 mixing ratio observed at Beltsville, Maryland at 04:08 and 12:46 local time (LT) on August 9, 2010. The PBL heights diagnosed using the LLJ nose location during nighttime and the 1.5-theta-increase method during daytime are marked using blue and red dashed horizontal lines, respectively.

Atmospheric static stability can be inferred by comparing θ_v profile with a vertical straight line in a θ_v profile plot, basically examining whether θ_v decreases or increases with height. Thus, θ_v inversion indicates a stable condition that is favorable for the accumulation of pollutants, while T inversion only include the extreme stable conditions since the slope of T profile in presence of T inversion is much larger than the dry-adiabatic lapse rate. Less stable conditions cannot be inferred by T inversion, and less-extreme stable condition may still occur even without a T inversion. Therefore θ_v profiles are more commonly used to diagnose the structure of PBL, including both static stability and PBL height, which is more straightforward than using T profiles given the ambiguity of T inversion and effectiveness of θ_v to infer stability. For dry air, profiles of θ are often used to examine PBL structure since the effect of moisture is minor.

The diurnal variation of PBL structure can be easily inferred from θ_v and/or θ profiles with the naked eye. In a stable boundary layer, θ_v and θ increase with height, while in a CBL, profiles of θ_v and θ generally exhibit a three-layered structure (Fig. 2A and D) with (1) a super-adiabatic unstable surface layer in which θ_v and θ decrease with height, (2) a near-neutral mixed layer in the middle where θ_v and θ vary little with height, and (3) a stably-stratified entrainment zone at the top with θ_v and θ rapidly increasing with height. A detailed examination of the slope of θ_v and θ profiles further reveals that the upper portion of CBL (above the neutral point at ~0.32 CBL height) is slightly static stable (Hu et al., 2019a). Such a structure is dictated by the different contribution of large eddies and small eddies in the CBL. Small eddies gradually transport heat from surface to upper CBL and lead to decreased θ with height, while non-local large eddies can deposit heat directly in the upper CBL and lead to a slightly stable θ profile.

In addition to thermodynamic structure/processes, dynamic structure of the PBL, including wind shear and mechanical turbulence, also affects the dispersion/transport processes of air pollutants and surface air quality, especially at night when convective eddies are not produced at the ground. Many previous studies (e.g., Klein et al., 2014) have reported that nighttime particulate matter and O_3 pollution were influenced by turbulence in presence of nocturnal low-level jets (LLJs). These PBL processes that often occur at night can either improve or worsen local surface air quality, depending on air quality in upstream regions and the vertical distribution of air pollutants.

Estimation of Boundary Layer Height

The PBL height is critical to air pollution meteorology since it dictates the dilution volume of pollutants. Many methods and instruments can be applied to estimate PBL heights (Zhang et al., 2020). The conventional and most reliable way to diagnose PBL heights is through analyzing radiosonde profiles using the critical bulk Richardson number method or the θ inversion identification method. One of the θ inversion methods defines the PBL height as the altitude where θ first exceeds the minimum θ within the PBL by 1.5 K. This method is also called the 1.5-theta-increase method. The θ inversion method is quite reliable to diagnose CBL height since a θ-inversion layer is always present at the top of CBL, whereas the presence of a T-inversion layer is not always guaranteed. This is another reason why θ profiles are more meaningful than T profiles in air pollution/boundary layer meteorology.

Unlike at the daytime CBL, it is difficult to estimate the PBL height according to thermal inversion during the night because θ-inversion is present through the entire depth of the nocturnal boundary layer. Instead, the nighttime PBL height can be better diagnosed using wind speed profiles. The nighttime PBL height is often determined as the altitude of the nose of the LLJ based on the inertial oscillation theory, according to which wind oscillation amplitude peaks at the top of the boundary layer.

In addition to radiosonde measurements, other observation techniques such as high-resolution infrared sounder, multi-channel microwave radiometer, sodar, and especially lidar were also applied to derive PBL height. The lidar-retrieved PBL height is usually marked as the altitude when the largest gradient in backscatter signal occurs. However, it can be easily affected by clouds and elevated aerosol plumes.

Take the radiosonde profiles at Beltsville, Maryland at 04:08 and 12:46 LT on August 9, 2010 (**Fig. 2**) as an example, profiles of θ_v and θ resembled each other in structure in daytime and nighttime (**Fig. 2**A and D). At daytime, profiles of θ_v and θ present a three-layered structure: a surface layer with θ_v and θ decreasing with height, a near-neutral mixed layer in the middle where θ_v and θ hardly vary with height, and a stably-stratified entrainment zone at the top with θ_v and θ rapidly increasing with height. However, a clearly defined boundary layer cannot be identified from the profile of T. T decreases all the way into the free troposphere without a clear transition at the top of the PBL. In theory, through comparing with a dry adiabatic lapse rate, PBL structure can be still diagnosed from T profile, however this is nearly impossible from visual inspection. In contrast, a prominent θ inversion is present in its profile, which reveals the top of the PBL. Thus, profile of θ (instead of T) should be used in any meaningful PBL discussions.

Based on the 1.5-theta-increase method, the PBL height is diagnosed at ~1.6 km near the bottom of the θ-inversion. The daytime PBL height well confines the dispersion of water vapor (**Fig. 2**E) and O_3 (**Fig. 2**F) in the PBL. Moisture accumulation and O_3 formation both predominantly occur in the PBL and both constituents show a sharp gradient at the top of the PBL. The daytime PBL height was far below from the bottom of the T-inversion at 2.5 km above the ground level in the free troposphere. Thus, this T-inversion has no implication for dispersion of constitutes such as water vapor and O_3.

During nighttime (4:08 a.m.) on August 9, 2010, using the LLJ nose method, the PBL height is estimated to be at 410 m (**Fig. 2**C), close to the bottom of the elevated T-inversion (**Fig. 2**B). Moisture was observed to accumulate within this stable boundary layer (**Fig. 2**E) and O_3 increased with height due to NO titration and dry deposition in the presence of weak turbulence (**Fig. 2**F).

Cases of Turbulent Mixing Dictating Air Pollution

Vertical mixing events are reported to affect the variation of O_3. **Fig. 3** shows observed O_3, NO_x, wind vector, temperature at Beltsville, Maryland on August 11, 2010. During the period from 1:00 to 4:00 LT, surface O_3 mixing ratio increased by about 30 parts per billion on a volume basis (ppbv) while NO_x mixing ratio decreased by ~25 ppbv (**Fig. 3**). During the night of August 10 and most of August 11, 2010 the air mass came from the north. A cold front passed the research site, traveling from north to south on August 11, 2010. If increases of O_3 resulted from the advection of an upstream polluted plume then mixing ratios of other pollutants such as CO, NO_x would likely be higher. However, NO_x level decreased as O_3 increased. The duration of this nocturnal O_3 increase (several hours) was similar to the "leaky inversion" event, which was caused by the vertical exchange of air between the surface stable boundary layer and the residual layer above. Since the residual layer had higher O_3 and lower concentrations of other pollutants, the vertical exchange of trace gases allowed decreases in surface NO_x and increases in surface O_3 (Hu et al., 2012).

Vertical mixing could be also induced from wind shear and impair air quality near the surface. Nighttime LLJs occur frequently in the Great Plains. The strong wind shear associated with LLJs was observed to affect the vertical redistribution of O_3. On the night of July 24–25, 2003 nocturnal O_3 maxima were noticed in the presence of an LLJ (**Fig. 4**). Such phenomenon occurred in Oklahoma quite frequently. Under calm conditions, surface O_3 normally decreased to very low levels ($< \sim$10 ppbv) between 20:00 and 22:00 LT due to dry deposition and NO titration (Klein et al., 2014). However, on the night of July 24–25, 2003 surface O_3 around OKC increased after 20:00 LT and O_3 concentration stayed at elevated levels (>40 ppbv) during most of the night. Such nocturnal O_3 maxima (or elevated O_3 concentration) were unlikely due to advection. On the nights of July 24–25, 2003 southerly wind persisted. If the nocturnal surface O_3 maxima were due to southerly advection of O_3-richer air mass, the upwind site, Goldsby would have experienced higher O_3 maxima than the other downwind sites, which was clearly not the case (**Fig. 4**). Instead, turbulence can be induced by the wind shear associated with the LLJs. Subsequent vertical mixing can transport O_3-richer air mass downward to the surface (Hu et al., 2013b), thus explaining the frequently observed nocturnal O_3 maxima associated with the LLJs.

In addition to O_3, vertical mixing also affects vertical distribution of aerosols. For instance, there was a diurnal variation in the monthly-averaged vertical profiles of PM_1, $PM_{2.5}$, and PM_{10} concentrations within 1.5 km above the surface in November 2018 in Shenyang, Northeast China (**Fig. 5**). On average, PM concentrations decreased with height at all hours. At night (02:00, 05:00, 20:00, and 23:00 LT), PM concentrations decreased rapidly with height below 500 m, with average vertical gradients of 5.8, 9.7, and 11.7 $\mu g\, m^{-3}$/100 m for PM_1, $PM_{2.5}$, and PM_{10}, respectively, and changed slowly aloft. In the daytime (08:00–17:00 LT),

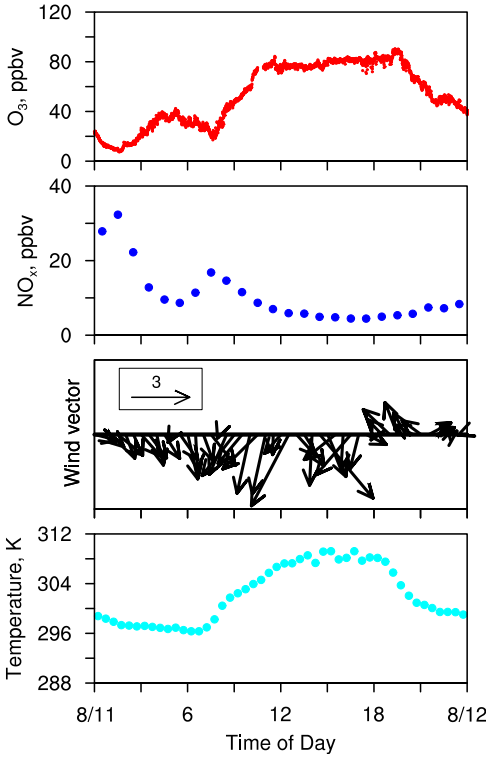

Fig. 3 Observed (top to bottom) O_3, NO_x, wind vector, temperature at Beltsville, Maryland on August 11, 2010.

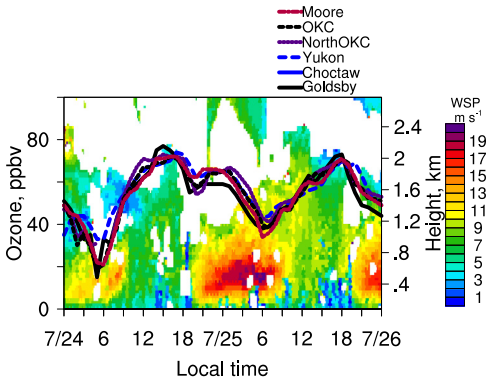

Fig. 4 Time-height diagram of wind speed in the atmospheric boundary layer and time series of surface O_3 observed on July 24–25, 2003 in the Oklahoma City (OKC) metropolitan area. The left Y-Axis is O_3 mixing ratio while the right Y-Axis is height for wind speed. The six EPA sites in the OKC metropolitan area where O_3 is observed are Moore, OKC, North OKC, Yukon, Choctaw, and Goldsby.

PM concentrations were distributed more uniformly in the vertical direction; the smallest concentration gradients of about 1.8, 3.0, and 3.8 μg m^{-3}/100 m below 500 m were observed at 14:00 LT for PM_1, $PM_{2.5}$, and PM_{10}, respectively. Aerosols were mostly distributed below 400 m at night, but were transported to higher altitudes (up to ~800 m) during the daytime by strong convective turbulence. The diurnal variation of PM vertical distributions is closely related to the diurnal evolution of PBL structures. Stronger atmospheric stability occurred at night in comparison to the daytime due to continuous radiative cooling of the surface after sunset, which suppressed vertical mixing of aerosols and trapped more aerosols near the surface. During the daytime, atmospheric stability became weak because of solar heating of the surface, which favored vertical transport of aerosols and resulted in a more uniform vertical distribution of PM concentrations (Li et al., 2019b). Observations and model results also revealed that nocturnal LLJs transported large amount of pollutants from the North China Plain to Shenyang. These pollutants were trapped in the residual layer during the previous night and then mixed to the surface after sunrise due to convective turbulence (Li et al., 2019a,b), causing surface aerosol pollution.

Vertical mixing may also be induced from cloud top radiative cooling and affect the variation of pollutants in the boundary layer. During the springtime, anomalously low O_3 mixing ratios are frequently observed in the Arctic region. Such phenomena are called

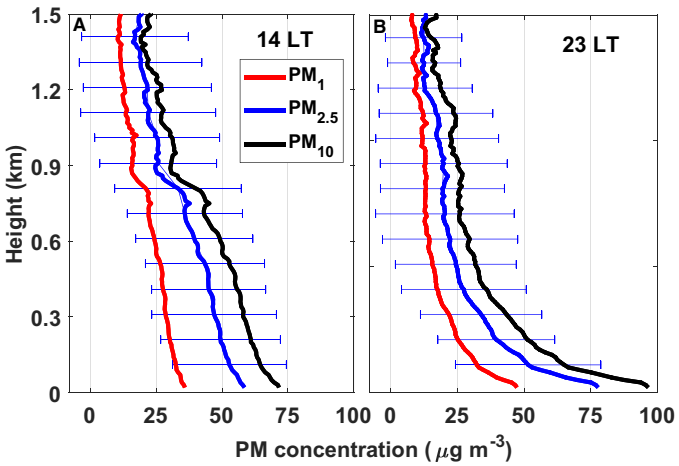

Fig. 5 Monthly averaged vertical profiles of PM_1, $PM_{2.5}$, and PM_{10} concentrations at (A) 14:00, and (B) 23:00 LT observed at Shenyang in November 2018. Blue bar represents the standard deviation of $PM_{2.5}$ concentration.

O_3 depletion events (ODEs). A few mechanisms are proposed to be responsible for the termination of the ODEs. One of the mechanisms is related to the vertical mixing induced from cloud top radiative cooling. Downdrafts and compensating updrafts induced by the cloud-top radiative cooling can be sufficiently strong to reach the surface. The averaged vertical velocity in the presence of clouds may be as large as 0.6 m s^{-1} in the mixed layer. The vertical mixing associated with updrafts and downdrafts triggered by the clouds can mix the free tropospheric O_3-richer air downward to replenish the O_3 near the surface, thereby terminating the ODEs (Hu et al., 2011). In midlatitude regions, cloud-top-induced turbulence is also reported to transport free-troposphere O_3 to the surface and thus lead to nocturnal surface O_3 peaks (Hu et al., 2021).

Cases of Advection Dictating Air Pollution

A good example of a favorable meteorological condition for heavy pollution is the horizontal advection induced by the coastal breeze in Los Angeles, California. The highly populated Los Angeles is surrounded by mountains on three sides and opens to the Pacific Ocean to the west and southwest. Pollutants accumulated over the urban areas in the stagnant morning air are regularly transported downwind with the onset of the westerly sea breeze in the morning. The air mass is moved back after the onset of land breeze in the evening. The back and forth flow of the air is constrained by the surrounding mountains which allows the air to become highly enriched with pollutants, which likely leads to pollution episodes. Land/sea breezes have also been reported to contribute to elevated O_3 events in other regions such as Houston, Texas and Hampton, Virginia. Lack of advection sometimes creates a "dead zone", leading to pollution episodes, such episodes were reported over Dallas in presence of Atlantic hurricane passages (Hu et al., 2019b).

Improvement of PBL Simulation

Uncertainties of PBL Schemes

The accuracy of air quality simulations is affected by the uncertainties associated with the model treatments for various processes, including vertical mixing, dry deposition and chemical reactions. Unresolved turbulent mixing within the PBL and the free troposphere is handled by the PBL scheme in the models. PBL schemes are therefore critical for reproducing the bulk boundary layer structures and profiles in the whole atmospheric column, as well as their subsequent effects on weather and air quality simulations. The uncertainties associated with the PBL schemes remain one of the main sources of inaccuracies in air quality simulations. Many studies (Hu et al., 2010a, 2012, 2013a, 2019a; Nielsen-Gammon et al., 2010; Wang and Hu, 2021) have evaluated the performance of various modern PBL schemes, with most of them focusing on continental cloud-free PBL. Compared to continental clear PBL, much less is known about the performance of PBL schemes in presence of clouds (Angevine et al., 2012; Huang et al., 2013; Yang et al., 2019). Also, most previous PBL modeling studies focus on treatments within the boundary layer while free-troposphere treatments rarely receive much attention (Hu et al., 2012; Zhu et al., 2021), likely because that free-troposphere turbulence is weak under clear conditions and the impact of its parameterization on weather and climate simulations is regarded as minor.

PBL schemes can be classified into local and nonlocal schemes. Local schemes estimate the turbulent fluxes at each point in a model from the mean atmospheric variables and/or their gradients at that point, whereas nonlocal schemes include turbulent fluxes based on the atmospheric variables and their variations over a deeper layer covering multiple model levels through the PBL (Cohen et al., 2015; Hu et al., 2010a). The assumption among local schemes that fluxes depend solely on local values and local gradients of model state variables is least valid under convective conditions when turbulent fluxes are dominated by large eddies

that transport fluid over longer distances (Hu et al., 2010a). Previous studies found that traditional local schemes (e.g., Mellor–Yamada–Janjić (MYJ) or quasi-normal scale elimination (QNSE)) predict daytime continental boundary layers that are too cool and shallow; while schemes that include non-local treatment, such as the Asymmetrical convective model, version 2 (ACM2, Pleim, 2007), the Yonsei University (YSU, Hong et al., 2006) schemes and the more recently-updated local scheme (e.g., Mellor–Yamada Nakanishi and Niino (MYNN, Nakanishi and Niino, 2006)) predict deeper and warmer daytime continental boundary layers than MYJ and QNSE (Bright and Mullen, 2002; Clark et al., 2015; Coniglio et al., 2013). Also, nonlocal PBL schemes can reproduce the slightly stable upper CBL (above the neutral point at ~0.32 CBL height) with proper treatment/partitioning between local and nonlocal fluxes, while local schemes often fail to do so (Hu et al., 2019a; Wang et al., 2016). The Shin-Hong nonlocal scheme with optimized nonlocal flux treatment (Shin and Hong, 2015) can reproduce the mean θ profile showing a slightly stable upper CBL derived from multi-year early afternoon radiosonde data over Beijing, China (Hu et al., 2019a).

Recent PBL developments are motivated by the drive toward a unified representation of both boundary layer and in-cloud turbulence, which has long been parameterized separately by PBL and cumulus schemes. Improved coupling between the boundary layer and cumulus clouds in unified schemes can be advantageous for modeling pollutant transport from the boundary layer to the free atmosphere through cloud venting (Ching 1981; Cotton et al., 1995). Most notably, a class of schemes known as the eddy-diffusivity mass-flux (EDMF) schemes synthesize the gradient-diffusion component from a PBL scheme with the mass flux model from a cumulus scheme to offer a unified parameterization of PBL turbulence and shallow cumulus convection (Soares et al., 2004; Angevine 2005; Siebesma et al., 2007; Pergaud et al., 2009; Angevine et al., 2010; Tan et al., 2018; Suselj et al., 2019), and has been extended to include deep convection (Suselj et al., 2022). Within the PBL, the mass flux term replaces the counter-gradient transport term to realize nonlocal transport. A recently developed MYNN-EDMF scheme by Olson et al. (2019) has revealed promising prospects in the simulation of shallow-cumulus-topped boundary layer (Angevine et al., 2018), which remains a challenge to numerical weather prediction and climate models. Besides EDMF schemes, the Cloud Layers Unified By Binormals (CLUBB) scheme is another recently-developed unified scheme for both PBL turbulence and clouds (Golaz et al., 2002a,b; Larson et al., 2012). CLUBB is essentially a higher-order turbulence scheme where subgrid-scale variability of vertical velocity, temperature and moisture are closed by assumed joint probability density functions. Despite its increased computational cost associated with solving higher-order moments, the CLUBB scheme is especially advantageous for its unified treatment of both cumulus and stratocumulus clouds, the latter do not fit well into the mass flux model.

Parameter Estimation

The accuracy of mode simulations is dictated by the uncertainties associated with model treatments for various processes. Parameter estimation offers a way to improve the accuracy of those model treatments. Parameter estimation is a technique for determining the best value of certain model parameters through data assimilation or similar techniques. When applied to parameterizations of meteorological processes, one hopes to identify optimal parameter values within a given parameterization, with "optimal" defined over some appropriate domain in space and time.

Advanced data assimilation methods, e.g., variational approaches and the ensemble Kalman filter (EnKF), are capable of extracting from observations significant information about the model parameters in addition to the model state. They have been used to counter model errors due to incorrect parameters by calibrating those parameters simultaneously with the model state during the analysis process. The EnKF was applied to estimate the flow-dependent optimal values of two parameters fundamental to the performance of a PBL scheme in the WRF model. Parameter-estimation EnKF results in a significant reduction in the model biases of both wind and temperature. Also, deterministic forecasts with updated parameters outperform forecasts with standard parameter settings (Hu et al., 2010c).

Ensemble Simulation

There are dramatic uncertainties in the air quality simulations due to uncertainties in the initial meteorological/chemical conditions and model treatments of physical and chemical processes. Even with plentiful observations, analysis inaccuracies are unavoidable, so a single-minded pursuit of improved initial conditions is inadvisable. Given the uncertainties associated with various model treatments under various conditions, improving model performance in a single deterministic simulation through pursuing perfect model treatments for all the conditions is also unlikely. Instead, ensemble simulations should be utilized to span the range of possible outcomes on a given day, and that uncertainty should be incorporated into the regulatory analysis (Thomas et al., 2019). An ensemble forecasting system, incorporating as many sources of error as possible, can provide guidance on not only the most likely pollutants evolution but also the range of possibilities.

Conclusion

Meteorological conditions play important roles in modulating air pollution through 1) modulating biogenic fluxes; 2) exerting influences on the formation and fate of pollutants; 3) dictating the dispersion/transport of pollutants. The planetary boundary layer (PBL) structure determines the mixing of pollutants and appropriate variables should be used to characterize PBL structure. Temperature (T) inversion does not work to infer boundary layer structure for both daytime and nighttime, potential temperature (θ)

should be used instead. θ profiles are more meaningful than T profiles in air pollution/boundary layer meteorology. Low-level jet nose can be used to diagnose nighttime boundary layer top according to the inertial oscillation theory.

Accurately simulating meteorological conditions is critical for simulating pollution events. Uncertainties are associated with model treatments for various processes in air quality models. Particularly an accurate PBL scheme is crucial for pollution simulation. Current status of PBL schemes is briefly surveyed and potential improvements through ensemble simulation and parameter estimation are discussed.

References

Angevine, W.M., 2005. An integrated turbulence scheme for boundary layers with shallow cumulus applied to pollutant transport. J. Appl. Meteorol. 44 (9), 1436–1452. https://doi.org/10.1175/JAM2284.1.

Angevine, W.M., Eddington, L., Durkee, K., Fairall, C., Bianco, L., Brioude, J., 2012. Meteorological model evaluation for CalNex 2010. Mon. Weather Rev. 140 (12), 3885–3906. https://doi.org/10.1175/Mwr-D-12-00042.1.

Angevine, W.M., Jiang, H.L., Mauritsen, T., 2010. Performance of an eddy diffusivity-mass flux scheme for shallow cumulus boundary layers. Mon. Weather Rev. 138 (7), 2895–2912. https://doi.org/10.1175/2010mwr3142.1.

Angevine, W.M., Olson, J., Kenyon, J., Gustafson, W.I., Endo, S., Suselj, K., Turner, D.D., 2018. Shallow cumulus in WRF parameterizations evaluated against LASSO large-eddy simulations. Mon. Weather Rev. 146 (12), 4303–4322. https://doi.org/10.1175/MWR-D-18-0115.1.

Bright, D.R., Mullen, S.L., 2002. The sensitivity of the numerical simulation of the southwest monsoon boundary layer to the choice of PBL turbulence parameterization in MM5. Weather Forecast. 17 (1), 99–114. https://doi.org/10.1175/1520-0434(2002)017<0099:Tsotns>2.0.Co;2.

Ching, J.K.S., 1981. The role of convective clouds in venting ozone from the mixed layer. Bull. Am. Meteorol. Soc. 62 (7), 1089–1089.

Clark, A.J., Coniglio, M.C., Coffer, B.E., Thompson, G., Xue, M., Kong, F.Y., 2015. Sensitivity of 24-h forecast dryline position and structure to boundary layer parameterizations in convection-allowing WRF model simulations. Weather Forecast. 30 (3), 613–638. https://doi.org/10.1175/Waf-D-14-00078.1.

Cohen, A.E., Cavallo, S.M., Coniglio, M.C., Brooks, H.E., 2015. A review of planetary boundary layer parameterization schemes and their sensitivity in simulating southeastern US cold season severe weather environments. Weather Forecast. 30 (3), 591–612. https://doi.org/10.1175/Waf-D-14-00105.1.

Coniglio, M.C., Correia, J., Marsh, P.T., Kong, F.Y., 2013. Verification of convection-allowing WRF model forecasts of the planetary boundary layer using sounding observations. Weather Forecast. 28 (3), 842–862. https://doi.org/10.1175/Waf-D-12-00103.1.

Cotton, W.R., Alexander, G.D., Hertenstein, R., Walko, R.L., McAnelly, R.L., Nicholls, M., 1995. Cloud venting - a review and some new global annual estimates. Earth Sci. Rev. 39 (3–4), 169–206. https://doi.org/10.1016/0012-8252(95)00007-0.

Golaz, J.-C., Larson, V.E., Cotton, W.R., 2002a. A PDF-based model for boundary layer clouds. Part I: method and model description. J. Atmos. Sci. 59 (24), 3540–3551. https://doi.org/10.1175/1520-0469(2002)059<3540:APBMFB>2.0.CO.

Golaz, J.-C., Larson, V.E., Cotton, W.R., 2002b. A PDF-based model for boundary layer clouds. Part II: model results. J. Atmos. Sci. 59 (24), 3552–3571. https://doi.org/10.1175/1520-0469(2002)059<3552:APBMFB>2.0.CO.

Hong, S.Y., Noh, Y., Dudhia, J., 2006. A new vertical diffusion package with an explicit treatment of entrainment processes. Mon. Weather Rev. 134 (9), 2318–2341. https://doi.org/10.1175/Mwr3199.1.

Hu, J., Hu, X.-M., Gao, L., Cai, C., Zhao, T., Zhang, X., 2021. Impacts of nocturnal cloud top radiative cooling on surface O3 in Sichuan basin, Southwestern China. Earth Space Sci. 8 (3), e2020EA001541. https://doi.org/10.1029/2020EA001541.

Hu, X.-M., 2008. Incorporation of the Model of Aerosol Dynamics, Reaction, Ionization, and Dissolution (MADRID) into the Weather Research and Forecasting Model with Chemistry (WRF/Chem): Model Development and Retrospective Applications (PhD thesis). NC State Univ. Retrieved from http://repository.lib.ncsu.edu/ir/handle/1840.16/5241.

Hu, X.-M., Doughty, D.C., Sanchez, K.J., Joseph, E., Fuentes, J.D., 2012. Ozone variability in the atmospheric boundary layer in Maryland and its implications for vertical transport model. Atmos. Environ. 46, 354–364. https://doi.org/10.1016/j.atmosenv.2011.09.054.

Hu, X.-M., Klein, P.M., Xue, M., 2013a. Evaluation of the updated YSU planetary boundary layer scheme within WRF for wind resource and air quality assessments. J. Geophys. Res. Atmos. 118 (18), 10490–10505. https://doi.org/10.1002/jgrd.50823.

Hu, X.-M., Klein, P.M., Xue, M., Zhang, F., Doughty, D.C., Forkel, R., Fuentes, J.D., 2013b. Impact of the vertical mixing induced by low-level jets on boundary layer ozone concentration. Atmos. Environ. 70, 123–130. https://doi.org/10.1016/j.atmosenv.2012.12.046.

Hu, X.-M., Nielsen-Gammon, J.W., Zhang, F.Q., 2010a. Evaluation of three planetary boundary layer schemes in the WRF model. J. Appl. Meteorol. Climatol. 49 (9), 1831–1844. https://doi.org/10.1175/2010jamc2432.1.

Hu, X.-M., Sigler, J.M., Fuentes, J.D., 2010b. Variability of ozone in the marine boundary layer of the equatorial Pacific Ocean. J. Atmos. Chem. 66 (3), 117–136. https://doi.org/10.1007/s10874-011-9196-z.

Hu, X.-M., Xue, M., Li, X., 2019a. The use of high-resolution sounding data to evaluate and optimize nonlocal PBL schemes for simulating the slightly stable upper convective boundary layer. Mon. Weather Rev. 147 (10), 3825–3841. https://doi.org/10.1175/mwr-d-19-0085.1.

Hu, X.-M., Xue, M., Kong, F.Y., Zhang, H.L., 2019b. Meteorological conditions during an ozone episode in Dallas-Fort Worth, Texas, and impact of their modeling uncertainties on air quality prediction. J. Geophys. Res. Atmos. 124 (4), 1941–1961. https://doi.org/10.1029/2018jd029791.

Hu, X.-M., Zhang, F., Nielsen-Gammon, J.W., 2010c. Ensemble-based simultaneous state and parameter estimation for treatment of mesoscale model error: a real-data study. Geophys. Res. Lett. 37, L08802. https://doi.org/10.1029/2010gl043017.

Hu, X.-M., Zhang, F., Yu, G., Fuentes, J.D., Wu, L., 2011. Contribution of mixed-phase boundary layer clouds to the termination of ozone depletion events in the Arctic. Geophys. Res. Lett. 38. https://doi.org/10.1029/2011gl049229.

Hu, X.M., Zhang, Y., Jacobson, M.Z., Chan, C.K., 2008. Coupling and evaluating gas/particle mass transfer treatments for aerosol simulation and forecast. J. Geophys. Res. Atmos. 113 (D11), D11208. https://doi.org/10.1029/2007jd009588.

Huang, H.Y., Hall, A., Teixeira, J., 2013. Evaluation of the WRF PBL parameterizations for marine boundary layer clouds: cumulus and stratocumulus. Mon. Weather Rev. 141 (7), 2265–2271. https://doi.org/10.1175/Mwr-D-12-00292.1.

Klein, P.M., Hu, X.M., Xue, M., 2014. Impacts of mixing processes in nocturnal atmospheric boundary layer on urban ozone concentrations. Boundary-Layer Meteorol. 150 (1), 107–130. https://doi.org/10.1007/s10546-013-9864-4.

Larson, V.E., Schanen, D.P., Wang, M., Ovchinnikov, M., Ghan, S., 2012. PDF parameterization of boundary layer clouds in models with horizontal grid spacings from 2 to 16 km. Mon. Weather Rev. 140 (1), 285–306. https://doi.org/10.1175/MWR-D-10-05059.1.

Li, X., Hu, X.-M., Ma, Y., Wang, Y., Li, L., Zhao, Z., 2019a. Impact of planetary boundary layer structure on the formation and evolution of air-pollution episodes in Shenyang, Northeast China. Atmos. Environ. 214, 116850. https://doi.org/10.1016/j.atmosenv.2019.116850.

Li, X., Ma, Y., Wang, Y., Wei, W., Zhang, Y., Liu, N., Hong, Y., 2019b. Vertical distribution of particulate matter and its relationship with planetary boundary layer structure in Shenyang, Northeast China. Aerosol Air Qual. Res. 19 (11), 2464–2476. https://doi.org/10.4209/aaqr.2019.06.0311.

Nakanishi, M., Niino, H., 2006. An improved Mellor—Yamada level-3 model: its numerical stability and application to a regional prediction of advection fog. Boundary-Layer Meteorol. 119 (2), 397—407. https://doi.org/10.1007/s10546-005-9030-8.
Nielsen-Gammon, J.W., Hu, X.-M., Zhang, F., Pleim, J.E., 2010. Evaluation of planetary boundary layer scheme sensitivities for the purpose of parameter estimation. Mon. Weather Rev. 138 (9), 3400—3417. https://doi.org/10.1175/2010mwr3292.1.
Olson, J.B., Kenyon, J.S., Angevine, W.A., Brown, J.M., Pagowski, M., Sušelj, K., 2019. A Description of the MYNN-EDMF Scheme and the Coupling to Other Components in WRF—ARW. NOAA Technical Memorandum OAR GSD; 61. https://doi.org/10.25923/n9wm-be49.
Shin, H.H., Hong, S.-Y., 2015. Representation of the subgrid-scale turbulent transport in convective boundary layers at gray-zone resolu- tions. Mon. Wea. Rev. 143, 250—271. https://doi.org/10.1175/MWR-D-14-00116.1.
Siebesma, A.P., Soares, P.M.M., Teixeira, J., 2007. A combined eddy-diffusivity mass-flux approach for the convective boundary layer. J. Atmos. Sci. 64 (4), 1230—1248. https://doi.org/10.1175/JAS3888.1.
Soares, P.M.M., Miranda, P.M.A., Siebesma, A.P., Teixeira, J., 2004. An eddy-diffusivity/mass-flux parametrization for dry and shallow cumulus convection. Q. J. R. Meteorol. Soc. 130 (604), 3365—3383. https://doi.org/10.1256/qj.03.223.
Suselj, K., Kurowski, M.J., Teixeira, J., 2019. A unified eddy-diffusivity/mass-flux approach for modeling atmospheric convection. J. Atmos. Sci. 76 (8), 2505—2537. https://doi.org/10.1175/JAS-D-18-0239.1.
Suselj, K., Smalley, M., Lebsock, M.D., Kurowski, M.J., Witte, M.K., Teixeira, J., 2022. Coupling warm rain with an eddy diffusivity/mass flux parameterization: 1. Model description and validation. J. Adv. Model. Earth Syst. 14 (8), e2021MS002736. https://doi.org/10.1029/2021MS002736.
Tan, Z., Kaul, C.M., Pressel, K.G., Cohen, Y., Schneider, T., Teixeira, J., 2018. An extended eddy-diffusivity mass-flux scheme for unified representation of subgrid-scale turbulence and convection. J. Adv. Model. Earth Syst. 10 (3), 770—800. https://doi.org/10.1002/2017MS001162.
Pergaud, J., Masson, V., Malardel, S., Couvreux, F., 2009. A parameterization of dry thermals and shallow cumuli for mesoscale numerical weather prediction. Bound. Layer Meteorol. 132, 83—106.
Pleim, J.E., 2007. A combined local and nonlocal closure model for the atmospheric boundary layer. Part I: model description and testing. J. Appl. Meteorol. Climatol. 46 (9), 1383—1395. https://doi.org/10.1175/Jam2539.1.
Thomas, A., Huff, A.K., Hu, X.-M., Zhang, F., 2019. Quantifying uncertainties of ground-level ozone within WRF-Chem simulations in the Mid-Atlantic region of the United States as a response to variability. J. Adv. Model. Earth Syst. 11 (4), 1100—1116. https://doi.org/10.1029/2018MS001457.
Wang, J.X., Hu, X.M., 2021. Evaluating the performance of WRF urban schemes and PBL schemes over Dallas-Fort worth during a dry summer and a wet summer. J. Appl. Meteorol. Climatol. 60 (6), 779—798. https://doi.org/10.1175/Jamc-D-19-0195.1.
Wang, W.G., Shen, X.Y., Huang, W.Y., 2016. A comparison of boundary-layer characteristics simulated using different parametrization schemes. Boundary-Layer Meteorol. 161 (2), 375—403. https://doi.org/10.1007/s10546-016-0175-4.
Yang, Y., Hu, X.-M., Gao, S., Wang, Y., 2019. Sensitivity of WRF simulations with the YSU PBL scheme to the lowest model level height for a sea fog event over the Yellow Sea. Atmos. Res. 215, 253—267. https://doi.org/10.1016/j.atmosres.2018.09.004.
Zhang, H., Wang, Y., Hu, J., Ying, Q., Hu, X.-M., 2015. Relationships between meteorological parameters and criteria air pollutants in three megacities in China. Environ. Res. 140, 242—254. https://doi.org/10.1016/j.envres.2015.04.004.
Zhang, H., Zhang, X., Li, Q., Cai, X., Fan, S., Song, Y., Zhu, T., 2020. Research progress on estimation of the atmospheric boundary layer height. J. Meteorol. Res. 34 (3), 482—498. https://doi.org/10.1007/s13351-020-9910-3.
Zhang, Y., Hu, X.M., Leung, L.R., Gustafson, W.I., 2008. Impacts of regional climate change on biogenic emissions and air quality. J. Geophys. Res. Atmos. 113 (D18), D18310. https://doi.org/10.1029/2008jd009965.
Zhu, P., Hazelton, A., Zhang, Z., Marks, F.D., Tallapragada, V., 2021. The role of eyewall turbulent transport in the pathway to intensification of tropical cyclones. J. Geophys. Res. Atmos. 126 (17), e2021JD034983. https://doi.org/10.1029/2021JD034983.

Further Reading

Stull, R.B., 1988. An Introduction to Boundary Layer Meteorology. Kluwer, Norwell, Mass.